Journal of Inorganic and General Chemistry
ZAAC
Zeitschrift für anorganische und allgemeine Chemie
DOI: 10.1002/zaac.202000314
ARTICLE

Transport Properties of Ag-doped ZnSb

Daniel Eklöf,[a] Andreas Fischer,[b] Jekabs Grins,[a] Wolfgang Scherer,[b] and Ulrich Häussermann*[a]

Dedicated to Professor Sven Lidin on the Occasion of his 60th Birthday

Abstract. The intermetallic compound ZnSb is a (II-V) narrow gap semiconductor with interesting thermoelectric properties. Electrical resistivity, Hall coefficient, thermopower and thermal conductivity were measured up to 400 K on Ag-doped samples with concentrations 0.2, 0.5, 1, 2, and 3 at.%, which were consolidated to densities in excess of 99.5 % by spark plasma sintering. The work confirms a huge improvement of the thermoelectric Figure-of-merit, *ZT*, upon Ag doping. The optimum doping level is near 0.5 at.% Ag and results in *ZT* values around 1.05 at 390 K. The improvement stems from a largely decreased resistivity, which in turn relates to an increase of the hole charge carrier concentration by two orders of magnitude. It is argued that Ag can replace minute concentrations of Zn (on the order of 0.2 at.%) in the crystal structure which enhances the intrinsic impurity band of ZnSb. Excess Ag was found to segregate in grain boundaries. So the best performing material may be considered as a composite $Zn_{\sim 0.998}Ag_{\sim 0.002}Sb/Ag_{\sim 0.003}$.

Introduction

The binary Zn-Sb system affords two narrow gap semiconductors phases, Zn_4Sb_3 and ZnSb, which are among the cheapest high-performance thermoelectric materials. Zn_4Sb_3 possesses an intrinsically disordered crystal structure[1–3] and has been intensively investigated.[4] The Figure-of-merit *ZT* for this material exceeds 1 above 500 K, and increases to almost 1.4 at 670 K.[5] *ZT* is defined as $(S^2/\rho\kappa)T$, where T is the absolute temperature, S the thermopower, ρ the electrical resistivity, and κ the thermal conductivity.

Like Zn_4Sb_3, ZnSb is a *p*-type material but its performance is somewhat inferior.[6,7] A major ingredient to understanding the thermoelectric properties of ZnSb is an acceptor impurity band, which possibly relates to a slight Zn-deficiency, $Zn_{1-\delta}Sb$.[8,9] Recent investigations on hot-pressed specimens showed *ZT* values around 0.8 at 550 K.[10] Higher Figures-of-merit (approaching 1 at 600 K) were achieved in composite materials containing 2.5 % Zn_3P_2 particles and 0.2 % Cu.[11] Further, numerous doping studies were performed, involving e.g. Cu, Sn, In, which could also produce *ZT* values around 1 at 600 K.[12–14]

Most remarkable, however, has been a report on Ag doping which increased *ZT* to 1.15 at 670 K, which is almost on par with Zn_4Sb_3.[15] In this work it was assumed that Ag dopant, which was added in molar concentrations 0.2 and 2 % to the Zn and Sb synthesis mixture, formed Ag_3Sb particles which then nanostructured with the embedding ZnSb matrix. The presence and distribution of Ag_3Sb nanoparticles in ZnSb was then made responsible for an optimized carrier concentration and a significant reduction in lattice thermal conductivity. Interestingly, a recent study on Ag-doped thin films of ZnSb confirmed the improved thermoelectric performance from the addition of Ag but could not find Ag_3Sb particles although similar doping concentrations (1–2 at.%) were applied.[16] Instead it was assumed that Ag would replace partially Zn as in a solid solution, $Zn_{1-x}Ag_xSb$.

Herein we present a detailed study of the transport properties of Ag-doped ZnSb, involving spark plasma sintered specimens with the nominal composition $Zn_{1.02}SbAg_x$, and x ranging from 0.2 to 3 at.%. The intention of the study was to unambiguously quantify the effect of Ag doping on thermoelectric properties and to find out about the faith of dopant Ag in ZnSb specimens.

Experimental Section

Synthesis: Bulk samples $Zn_{1.02}Sb_1Ag_x$ with x = 0.2. 0.5, 1, 2, and 3 at.% were prepared from mixtures of the elements (Zn shots (99.99 %, ACBR), Sb shots (99.999 %, ACBR), dendritic Ag (ABCR, 99.999 %)). Weighed mixtures of batches with a total mass of about 2.2 g were loaded in fused silica ampoules which were flame sealed in a dynamic vacuum ($<10^{-5}$ bar). The ampoules were placed upright in a resistance box furnace and heated overnight at 800 °C. The following day, ampoules were shaken inside the furnace vigorously three times, with 5 min intervals, and then left to rest for 20 min prior to quenching in water. The obtained intermetallic ingots were ground into a fine powder in an agate mortar inside an Ar filled glove box. The powder was then pressed into pellets, which were sealed in a fused silica ampoule and subsequently annealed for 5 days at 510 °C.

Processing: The annealed pellets were ground into a fine, micron-sized, powder and loaded into a graphite die (diameter 12 mm), being part of a SPS 530ET (Dr. Sinter Spark Plasma Sintering System, Fuji

* Prof. Dr. U. Häussermann
E-Mail: Ulrich.Haussermann@mmk.su.s
[a] Department of Materials and Environmental Chemistry
Stockholm University
10691 Stockholm, Sweden
[b] Institute of Physics
Augsburg University
86159 Augsburg, Germany

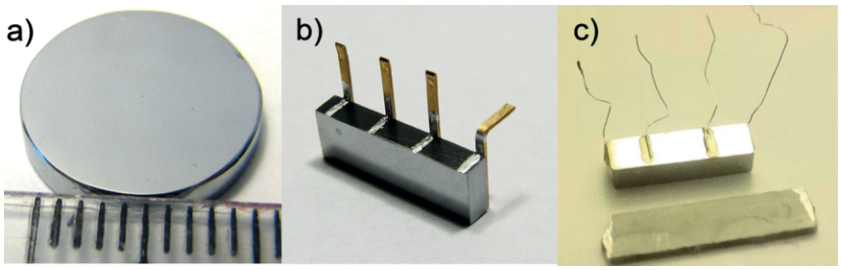

Figure 1. (a) Photograph of a spark plasma sintered ZnSb specimen after polishing, scale division is 1 mm. (b) Wire-cut piece as prepared for a TTO measurement in the PPMS. The bent leg is the cold foot and ground. (c) Wire-cut pieces as prepared for 4-point resistivity measurements (top, 0.05 mm Pt wires attached) and Hall measurements (bottom, without Pt wires (in total 5 would be attached: 2 at the short edges (as for resistivity), two at the lower long side and one at the upper long side). The sample material was $Zn_{1.02}SbAg_{0.005}$.

Electronic Industrial Co. Ltd, Japan) spark plasma sintering instrument. This instrument is located inside an argon-filled glovebox, so all steps of synthesis – as described above – and sintering were done uninterruptedly under air-free conditions. The powder was covered with a graphite fiber sheet to avoid direct contact between the powder compact and the graphite die. A heating rate of 50 K/min was applied and samples were sintered at 450 °C for 15 min at a pressure of 75 MPa. The heat increment was maintained by using a pulsed DC. The sintering temperature was measured by a K-type thermocouple placed in the graphite die about 2 mm away from the sample. The initially applied pressure was 20 MPa and gradually increased with increasing temperature. The maximum pressure of 75 MPa was applied when the sample temperature had reached 430 °C. The sintered samples had a thickness of 2 mm (and a diameter of ca. 11 mm) after removing the graphite layer by polishing and displayed a shiny metallic luster (Figure 1a). Thereafter sintered samples were cut into smaller pieces with defined geometries using a wire saw. These pieces were used for further investigations and analysis, as described below. The remaining parts of pellets after cutting were ground and used for powder X-ray diffraction.

Sample Analysis: Powder X-ray diffraction (PXRD) patterns were collected on a Panalytical X'Pert PRO diffractometer operated with Cu-$K_{\alpha 1}$ radiation and in θ-2θ diffraction geometry. Powder samples were applied to a zero diffraction plate and diffraction patterns measured in a 2θ range 20–90°. ZnSb materials were characterized as synthesized and after processing. Rietveld analysis was performed using the Fullprof Suite v2.05.[17] Scanning electron microscopy (SEM) investigations were performed on a JEOL JSM-7000F instrument to examine the microstructure and compositional homogeneity of ZnSb specimens. Samples (with sizes 2 × 2 × 2 mm) were first polished mechanically and then with an Ar^+ ion beam in a Cross Section Polisher SM-09011 instrument from JEOL. Backscattered electron images were recorded with an acceleration voltage of 8 kV. According to a simulation of the electron trajectory (program CASINO v2.48)[18] this voltage yields an information depth of 75–100 nm. For energy dispersive X-ray spectrometry (EDX) a X-ray detector from Oxford instruments, INCA X-sight, was used.

For TEM investigations a 2 × 2 mm sized sample was prepared by ion milling. First, the sample thickness was reduced to about 45 µm by mechanical polishing using diamond paper. The thin sample was then transferred and glued to a copper grid with a 1 × 2 millimeter hole. Thereafter it was milled at a 15° angle from the horizontal plane, with one Ar^+ ion beam from above and one from below. The sample was rotated during milling and cooled with liquid nitrogen.

The density of samples after sintering was determined by measuring volumes of ca. 2 × 2 × 2 mm pieces with a gas (He) expansion pycnometer (AccuPyc 1330 from MicroMeritics). The instrument was well calibrated and its accuracy confirmed with pieces of semiconductor grade crystalline Si of similar volume as the ZnSb samples. Errors in determined densities are estimated to 0.2 %.

Transport Measurements: Thermal and electronic transport measurements were performed in a temperature range 2–400 K (and occasionally between 100 and 400 K) using a Physical Property Measurement System (PPMS) from Quantum Design.

Thermopower and thermal conductivity were measured using a four-point contact setup in the Thermal Transport Option (TTO) mode of the PPMS. The sample dimension was 2 × 4 × 10 mm (cf. Figure 1b). Copper leads were glued on the sample via silver-filled epoxy (Epotek H31E) and measurements were done in high vacuum (10^{-6} bar). At a certain temperature, a heat pulse was applied to the sample to create a temperature gradient. Thermal conductivity and thermopower were obtained when the sample was equilibrated. The PPMS autorange feature was used in all measurements. Radiation heat loss was automatically corrected with the incorporated functions of the software. The error estimated for the thermopower is +/– 5 % due to broad contact leads, whereas for the thermal conductivity an error of about 10 % below 300 K and up to 25 % above 300 K is assumed due to thermal radiation effects.

The electrical resistivity measurements were performed by a four-point low frequency AC (7 Hz) method. Platinum wires (0.05 mm diameter) were connected to the samples using silver paint. The sample dimension was ca. 1 × 2 × 9 mm (cf. Figure 1c). Due to the irregular shape of these specimens, the sample cross section was estimated from the approximate average value across the sample. Therefore errors of up to 20 % in the absolute resistivity values may be assumed. Hall measurements were done in the AC transport mode of the PPMS. The sample (cf. Figure 1c) was contacted with 0.05 mm platinum wires and silver paint in a 5-point configuration using a potentiometer to minimize the resistance contributions to actual Hall voltage. Depending on sample geometry, a magnetic field between 1 and 3 T was applied perpendicular to the sample and a constant AC current of 50 mA and 107 Hz was used throughout the whole measurement.

Results and Discussion

When synthesizing Zn-Sb intermetallics it is important to recognize that Zn is rather volatile. Using stoichiometric reaction mixtures Zn:Sb = 1:1 for the synthesis of ZnSb will frequently result in the presence of 2–5 wt.% Sb impurity.[7,15,19,20] According to our experience (and referring to the synthesis procedure we applied), roentgenographically pure

samples of ZnSb can be obtained when using a slight, 2 at.%, excess of Zn, i.e. a nominal composition $Zn_{1.02}Sb$. This is shown with the Rietveld plot in Figure 2a. Accordingly, Ag doped samples were prepared by adding 0.2, 0.5, 1.0, 2.0, 3.0 at.% Ag to synthesis mixtures with composition $Zn_{1.02}Sb$. Further, it is important to point out that the density of our SPS consolidated Ag-doped samples was > 99.5 %, i.e. fully dense specimens were obtained. This is different to the previous study by Xiong et al., which was based on hot pressured sample specimens with densities between 93 and 98 %.[15]

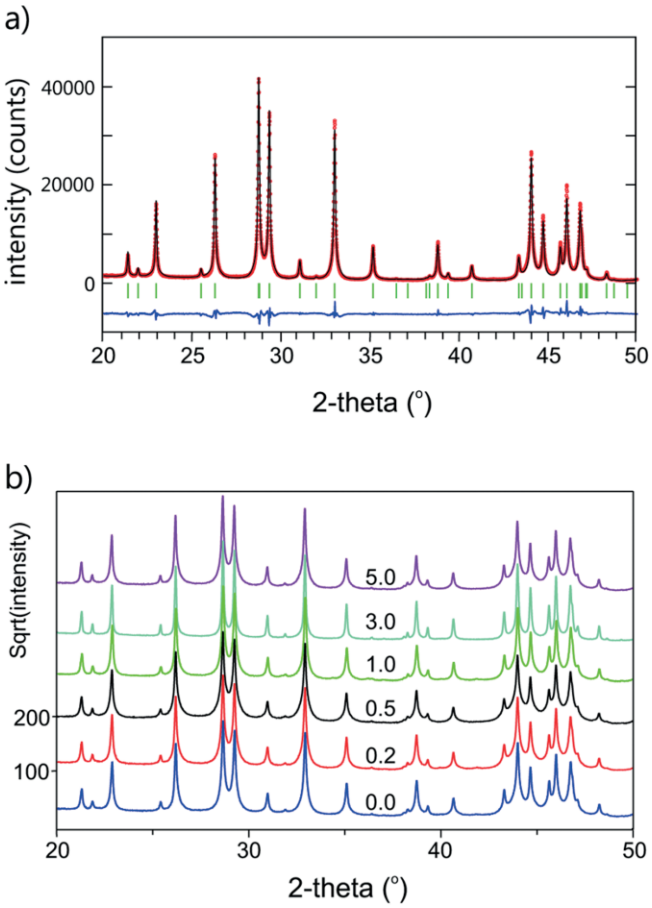

Figure 2. (a) Observed (red circles), calculated (black line) and difference (blue line) PXRD pattern for ZnSb from a structure refinement using the Rietveld method and 2θ = 20–50°. (b) PXRD patterns for undoped and Ag-doped ZnSb, with intensities on a square-root scale.

Figure 2b compares the PXRD pattern of ZnSb with the ones of the Ag-doped samples. The latter ones are virtually indistinguishable from ZnSb and the slight variations of the lattice parameters are not significant (see compilation, Table 1). Structure refinements using the Rietveld method resulted in R_F values of 2.6–4.2 % and χ^2 values of 6–13. The slightly high values of χ^2 can be attributed to both the good counting statistics and a difficulty of describing the very pronounced Lorentzian peak shapes. The substitution of Zn by Ag ($Zn_{1-x}Ag_xSb$) is expected to result in an increased unit cell volume, as the atomic volume of Ag (17.05 Å^3 per atom) is about 10 % larger than that of Zn (15.2 Å^3 per atom). For our samples, lattice parameter variations do not allow to draw any conclusion whether this is the case. Another important observation is that the PXRD patterns of all Ag-doped samples were not only void of impurity peaks from Zn_4Sb_3, ZnO, and Sb, but also of those related to Ag-Sb and Ag-Zn compounds. This is in contrast with the earlier report by *Xiong* et al. who spotted the presence of Ag_3Sb in the PXRD pattern of their 2.0 at.% Ag-doped sample.[15] This is also in contrast with a recent study on Ag-doped Zn_4Sb_3 where the presence of Ag_5Zn_8 was detected in samples doped as low as 0.5 at.% Ag.[21]

Table 1. Unit cell parameters for undoped and Ag-doped ZnSb, obtained from structure refinements using the Rietveld method.

Ag /at.%	*a* /Å	*b* /Å	*c* /Å	*V* /Å^3
0.0	6.2046(5)	7.7459(6)	8.1004(6)	389.293(5)
0.2	6.2050(4)	7.7471(6)	8.0990(7)	389.324(5)
0.5	6.2046(7)	7.7480(9)	8.0988(9)	389.336(8)
1.0	6.2043(4)	7.7472(5)	8.0997(5)	389.314(4)
2.0	6.2051(1)	7.7461(2)	8.1000(2)	389.326(2)
3.0	6.2046(6)	7.7475(7)	8.0993(8)	389.332(6)

Figure 3 compiles the results from the TTO measurements for the temperature range 100 to 400 K. As initially mentioned, it is well established that ZnSb is a *p*-type material where holes represent the majority charge carriers. Most noticeable is the drastic influence of Ag doping to the electrical resistivity. There is a significant reduction, by an order of magnitude, when comparing the 0.2 % and 2 % Ag samples, which have the highest and lowest resistivity, respectively (Figure 3a). There is no obvious trend between Ag concentration and temperature dependence of the resistivity. The 0.5 % and 3 % Ag samples display a very similar trend, with values between those of the 1 % and 2 % Ag samples. Notably, all doped samples display a shallow minimum in their resistivity vs. *T* behavior in the 320–330 K range. Also the thermopower varies significantly and irregularly (Figure 3b). Generally, Ag doping significantly reduces the thermopower (see discussion below), but there are also significant differences between the doped samples, with ZnSb-0.5 and ZnSb-1 %Ag displaying higher values than ZnSb-0.2, ZnSb-2, and ZnSb-3 %Ag.

The thermal conductivity is very similar for the doped samples, but values are 20–30 % higher than undoped ZnSb for which κ attains a value around 1.5 W·K^{-1}·m^{-1} at 300 K (Figure 3c). The thermal conductivity, κ, is composed of an electronic (κ_e) and lattice part (κ_L) and the increased values for the doped samples are attributed to the electronic component because of the increased carrier concentration (cf. discussion below). It is important to stress that the lattice thermal conductivity of ZnSb is actually very low. For temperatures above 100 K κ_L compares very well to bulk PbTe which is a state-of-the-art thermoelectric material.[22] The low lattice thermal conductivity of ZnSb has been attributed to a peculiar phonon structure, which in turn is a consequence of multicenter bonded structural entities in the crystal structure of ZnSb.[23] We find an optimum doping situation for 0.5 % Ag. *ZT* values of ca. 1.05 were obtained for ZnSb-0.5 %Ag at 390 K (Figure 3d). This is indeed a remarkable improvement compared to undoped ZnSb. It also significantly exceeds the *ZT* values of *Xiong* et al.'s 0.2 % Ag-doped ZnSb sample and state-of-the

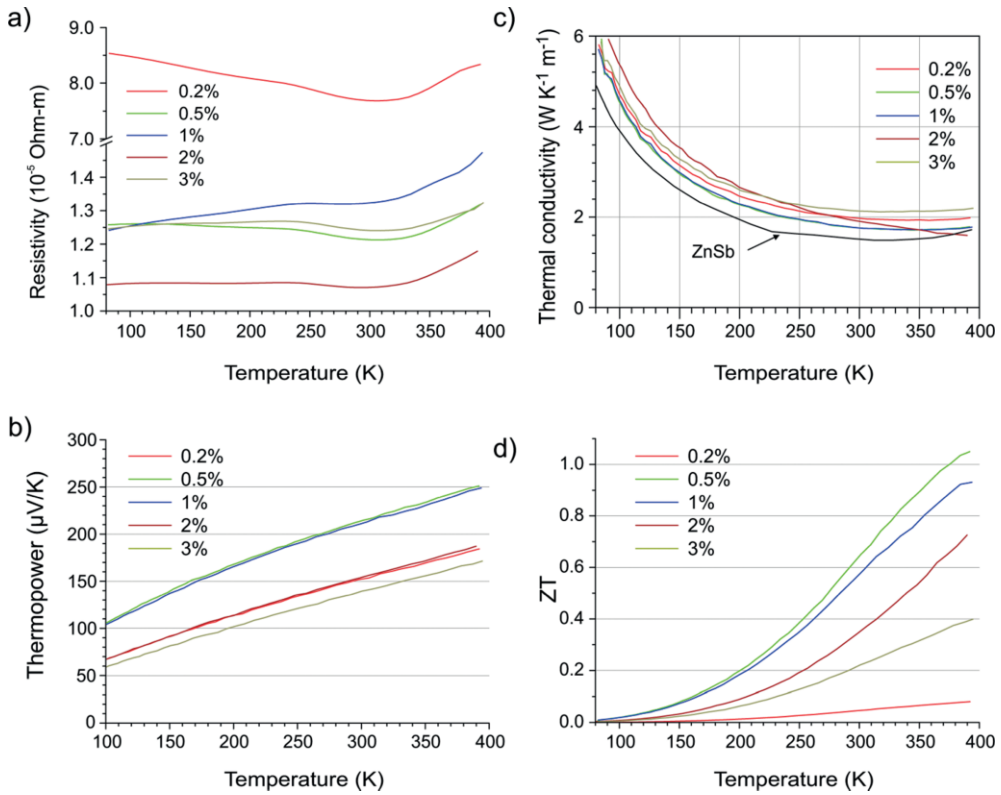

Figure 3. (a) Electrical resistivity, (b) thermopower, (c) thermal conductivity, and (d) dimension less Figure-of-merit *ZT* for Ag-doped ZnSb in a temperature range of 100–400 K (TTO measurements).

art $(Zn_{0.9925}Ag_{0.0075})_4Sb_3$ which are 0.75 and 0.8, respectively, at this temperature.[15,21]

Figure 4 compares specifically the resistivity and thermopower changes between undoped ZnSb and the optimally doped sample with 0.5 % Ag, now also considering low temperatures down to 2 K. Resistivity measurements were performed with the ACT option of the PPMS and are in good agreement with the TTO measured ones. Note that the thermopower of undoped ZnSb specimens can be very high, above 600 μV·K^{-1} at 300 K, when the Zn defect concentration is low.[24] The thermopower is decreased by about 50 % for the optimally doped sample, which indicates a vastly higher charge carrier concentration compared to undoped ZnSb. The *T* dependence of the resistivity for undoped ZnSb is governed by an impurity band. This has been earlier recognized by *Justi* et al.[25] and lately reinvestigated by *Song* et al.[9] The acceptor (impurity) band is located above the valence band with a small activation energy (< 0.1 eV). The resistivity behavior at low temperatures (up to 50 K) is then explained by the population of this acceptor band when k_BT becomes larger than the activation energy. In the quasi-linear range, from 50 K to 350–400 K, the impurity band is completely occupied and the concentration of carriers is constant with temperature (exhaustion range). Finally, intrinsic conductivity occurs at high temperature with the excitation of electrons across the forbidden gap, which has a size of about 0.5 eV.[26] The onset of intrinsic conductivity also involving electrons is detrimental to thermopower.[25] Compared with undoped ZnSb, resistivity values are decreased by an order of magnitude in the 0.5 % Ag doped sample. Further, the temperature dependence of the resistivity curve appears changed. The maximum at around 350 K, which for undoped ZnSb marks the onset of intrinsic conduction, is absent for doped samples, but may be expected at higher temperatures. The origin of the minimum at around 320 K, which has been mentioned earlier (cf. Figure 3a), is not clear.

Some more information can be extracted from the Hall measurements, Figure 5. For undoped ZnSb the charge carrier density, CC = $1/R_H$, is about 2×10^{17}/cm^3 in the exhaustion range and increases steeply when intrinsic conductivity takes place above 350 K (however, note that the formula CC = $1/R_H$ is not valid for the bipolar conductor situation above 350 K). As seen in Figure 5b, when adding Ag the CC increases by two orders of magnitude. This is already the case for lightly doped ZnSb-0.2 %Ag. For ZnSb-0.5 %Ag the CC is about 4.5×10^{19}/cm^3 which exceeds the optimum CC of about 2×10^{19}/cm^3 as calculated by *Böttger* at al.[8] Further, for ZnSb-0.2 %Ag and ZnSb-0.5 %Ag the CC increases with increasing temperature, as expected for a semiconductor. When more Ag is added, the temperature dependence changes sign and for ZnSb-1.0 %Ag the CC decreases with increasing temperature. This indicates that both holes and electrons are present, i.e. ZnSb-1.0 %Ag changed to a bipolar semiconductor.

Recently *Song* et al. speculated that the impurity acceptor band of ZnSb could connect to a sizeable concentration of native point defects.[9] This hypothesis has been corroborated by theoretical work where very low formation energies for Zn

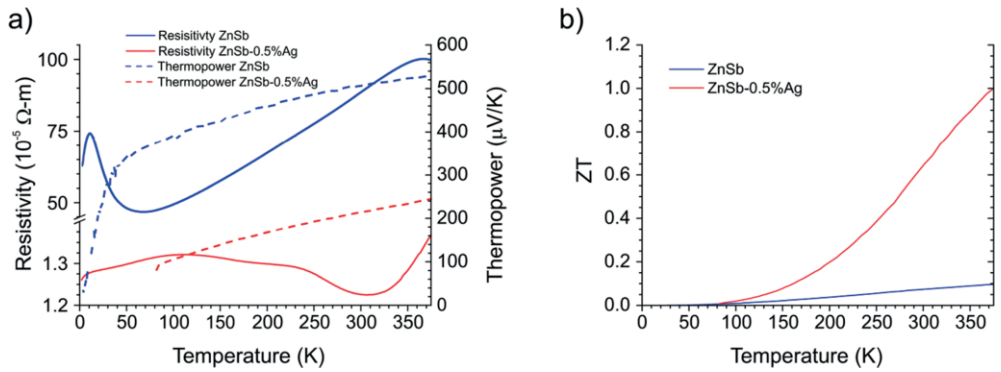

Figure 4. Comparison of (a) resistivity (ACT measurement) and thermopower for undoped ZnSb and optimally doped ZnSn-0.5 %Ag and (b) their Figure-of-merit.

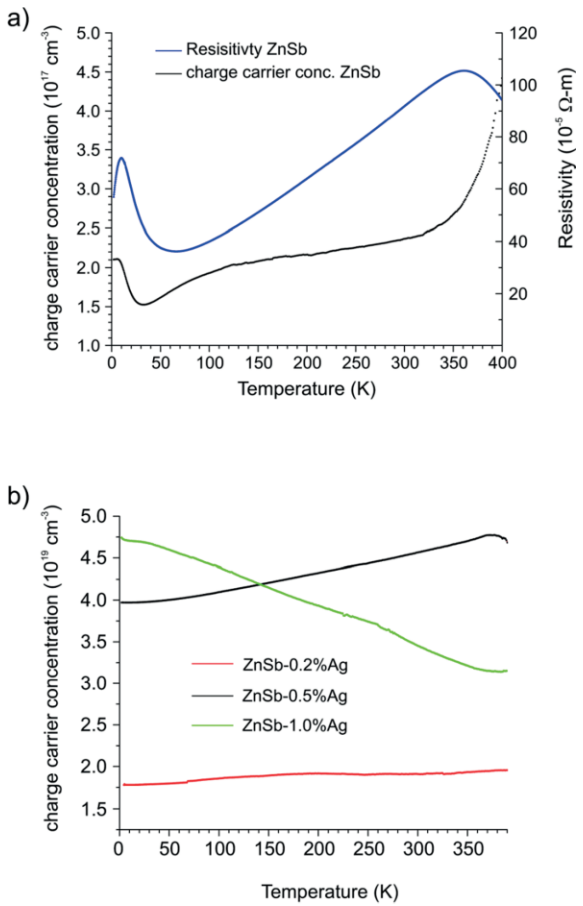

Figure 5. (a) Resistivity and charge carrier density for undoped ZnSb in the temperature range 2–400 K. (b) Charge carrier density for 0.2, 0.5, 1 %-Ag according to CC = $1/R_H$.

point defects (0.3–0.8 eV, depending on the defect charge) were established.[27,28] It appears that Ag doping enhances the impurity band of ZnSb, yet the mechanism is not clear. One may assume that small concentrations of monovalent Ag replace divalent Zn in the crystal structure, as in a solid solution $Zn_{1-x}Ag_xSb$. This has been proposed for Ag-doped thin films of ZnSb and also suggested for Zn_4Sb_3 (i.e. $(Zn_{1-x}Ag_x)_4Sb_3$) for which an optimum doping situation was found when employing a synthesis mixture $(Zn_{0.9925}Ag_{0.0075})_4Sb_3$.[21] Effective doping of ZnSb takes place already for 0.2 at.% Ag, which implies that x attains very low values (which we estimate to be in a range 0.001–0.002). "Over"-doping, as indicated in bipolar conduction for the sample ZnSb-1.0 %Ag, may introduce a donor impurity band. Note that properties for Ag-doped Zn_4Sb_3 are changed in a different way, indicating that the doping mechanism is rather different compared to ZnSb. The CC of undoped β-Zn_4Sb_3 is already high, 6.6×10^{19}/cm^3 at room temperature, and increases just by a factor of 2 for optimally doped $Zn_{0.9925}Ag_{0.0075}Sb$. This results in a decrease of the resistivity by a similar factor and, interestingly, in an increase of the thermopower by about 20 %.[21]

The small concentrations of potentially alloyed Ag in ZnSb will not manifest themselves in a change of the lattice parameters or unit cell volume of ZnSb (cf. Figure 2b). Furthermore, these small concentrations cannot be detected reliably by EDX analysis. As a matter of fact, despite exhaustive SEM and TEM investigations, it was not possible to obtain conclusive information about the faith of Ag in the Ag-doped ZnSb samples. Figure 6 shows a collection of SEM figures. Figure 6a depicts the grain structure of undoped ZnSb. The sample is completely dense and grain sizes vary from submicron to about 10 microns. The variation of gray scale is due to grain orientation and/or slight variations in Zn concentration, i.e. $Zn_{1-\delta}Sb$. Figure 6b shows the 0.5 % Ag doped sample. The black spots are associated with occasional voids and the white parts indicate Ag-rich domains which are located as submicron sized particles in the grain boundaries and possibly as nano-meter sized inclusions interspersed in the ZnSb grains. We were not able to conclusively determine (from both SEM and also TEM investigations) whether these particles correspond to pure Ag, or to Ag_3Sb. Figure 6c shows the 2 % Ag doped sample. It was hoped that the larger Ag concentration would allow a more conclusive picture. However, this sample looked very similar to the 0.5 % Ag doped one. In conclusion, we infer that small concentrations of Ag (on the order of 0.1–0.2 at.%) can replace Zn and by this influences (enhances) the impurity band of ZnSb. The optimum doping concentration was around 0.5 % Ag, and excess Ag (beyond 0.1–0.2 at.%) was found accumu-

lated (mostly) in grain boundaries. So these materials would represent composites of $Zn_{\sim 0.998}Ag_{\sim 0.002}Sb$ and Ag.

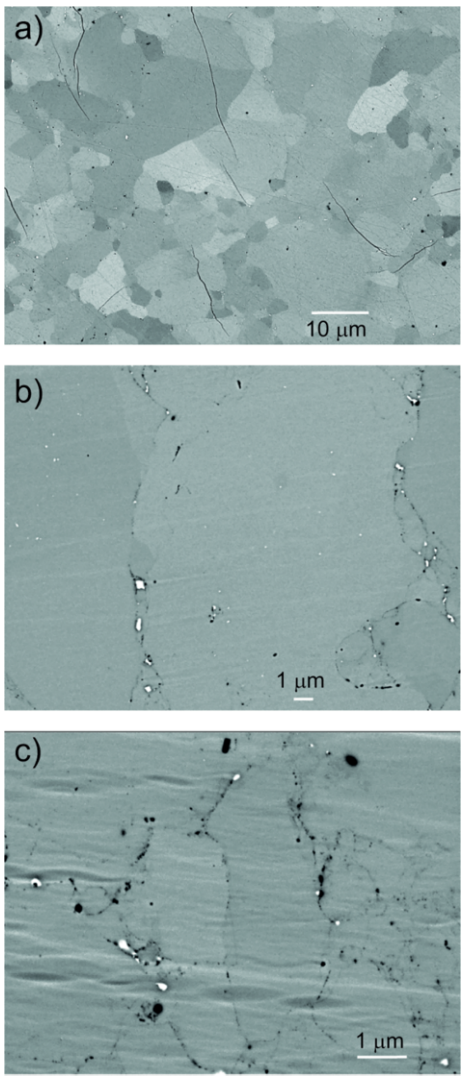

Figure 6. (a) SEM backscattered electron images for undoped ZnSb, (b) ZnSb-0.5 %Ag, and (c) ZnSb-2.0 %Ag. White areas are elemental Ag or possibly Ag_3Sb and black areas correspond to pores. The acceleration voltage was 8 kV and the information depth is estimated to 75–100 nm.

Conclusions

The transport properties of Ag doped samples of ZnSb were determined and a largely improved thermoelectric Figure-of-merit could be confirmed. The improvement is due to a considerably decreased resistivity, which in turn relates to a drastic increase of the charge carrier concentration by two orders of magnitude, from 10^{17} cm^{-3} to 10^{19} cm^{-3}. Already small concentrations of Ag (0.2 at.%) would show this effect and optimum doping was established at around 0.5 at.% Ag. It is conjectured that Ag doping enhances the acceptor impurity band, which is inherent to ZnSb, by increasing the number of acceptor states and shifting the transition to intrinsic conduction – which is detrimental to thermoelectric properties – to higher temperatures. The mechanism for this, however, remains unclear. It is likely that small concentrations of Ag can replace Zn in the crystal structure of ZnSb, but this was not detectible by the available analysis methods. Excess Ag was found to be accumulated in grain boundaries.

Acknowledgements

This work was supported by the Swedish Research Council under contract number 2013–4690, the National Science Foundation through grant DMR-1007557 and the Deutsche Forschungsgemeinschaft (SCHE 487/12–1).

Keywords: Intermetallic phases; Zinc antimonide; Zinc; Antimony; Thermoelectric properties

References

[1] G. J. Snyder, M. Christensen, E. Nishibori, T. Caillat, B. B. Iversen, *Nat. Mater.* **2004**, *3*, 458–463.
[2] J. Nylén, M. Andersson, S. Lidin, U. Häussermann, *J. Am. Chem. Soc.* **2004**, *126*, 16306–16307.
[3] J. Nylén, S. Lidin, M. Andersson, B. B. Iversen, H. Liu, N. Newman, U. Häussermann, *Chem. Mater.* **2007**, *19*, 834–838.
[4] B. B. Iversen, *J. Mater. Chem.* **2010**, *20*, 10778–10787.
[5] T. Caillat, J.-P. Fleurial, A. Borshchevsky, *J. Phys. Chem. Solids* **1997**, *58*, 1119–1125.
[6] M. I. Fedorov, L. V. Prokofieva, D. A. Pshenay-Severin, A. A. Shabaldin, P. P. Konstantinov, *J. Electron. Mater.* **2014**, *43*, 2314–2319.
[7] X. Song, T. G. Finstad, INTECH http://dx.doi.org/10.5772/65661.
[8] P. H. M. Böttger, G. S. Pomrehn, G. J. Snyder, T. G. Finstad, *Phys. Status Solidi A* **2011**, *208*, 2753–2759.
[9] X. Song, P. H. M. Böttger, O. B. Karlsen, T. G. Finstad, J. Taftø, *Phys. Scr.* **2012**, *T148*, 014001.
[10] C. Okamura, T. Ueda, K. Hasezaki, *Mater. Trans.* **2010**, *51*, 860–862.
[11] K. Valset, P. H. M. Böttger, J. Tafto, T. G. Finstad, *J. Appl. Phys.* **2012**, *111*, 023703.
[12] M. I. Fedorov, L. V. Prokofieva, Yu. I. Ravich, P. P. Konstantinov, D. A. Pshenay-Severin, A. A. Shabaldin, *Semiconductors* **2014**, *48*, 432–437.
[13] A. A. Shabaldin, L. V. Prokofieva, G. J. Snyder, P. P. Konstantinov, G. N. Isachenko, A. V. Asach, *J. Electron. Mater.* **2016**, *45*, 1871–1874.
[14] K. Valset, X. Song, T. G. Finstad, *J. Appl. Phys.* **2015**, *117*, 045709.
[15] D.-B. Xiong, N. L. Okamoto, H. Inui, *Scripta Mater.* **2013**, *69*, 397–400.
[16] L. Song, J. Zhang, B. B. Iversen, *ACS Appl. Energy Mater.* **2020**, *3*, 2055–2062.
[17] J. Rodríguez-Carvajal, Fullprof: A Program for Rietveld Refinement and Pattern Matching Analysis, Abstract of the Satellite Meeting on Powder Diffraction of the *XV Congress of the IUCr*, Toulouse, France 1990, p 127.
[18] Program Casino (Monte Carlo Simulation of electron trajectory in solids) v2.48. [http://www.gel.usherbrooke.ca/casino/index.html].
[19] A. B. Blichfeld, B. B. Iversen, *J. Mater. Chem. C* **2015**, *3*, 10543–10553.
[20] Q. Guo, S. Luo, *Funct. Mater. Lett.* **2015**, *8*, 1550028.
[21] L. Song, A. B. Blichfeld, J. Zhang, H. Kasai, B. B. Iversen, *J. Mater. Chem. A* **2018**, *6*, 4079–4087.

[22] D. Eklöf, A. Fischer, Y. Wu, E. W. Scheidt, W. Scherer, U. Häussermann, *J. Mater. Chem. A* **2013**, *1*, 1407–1414.
[23] A. Fischer, E. W. Scheidt, W. Scherer, D. E. Benson, Y. Wu, D. Eklöf, U. Häussermann, *Phys. Rev. B* **2015**, *91*, 224309.
[24] K. J. Hettwer, E. Justi, G. Schneider, *Adv. Energy Convers.* **1965**, *5*, 355–363.
[25] E. Justi, W. Rasch, G. Schneider, *Adv. Energy Convers.* **1964**, *4*, 27–38.
[26] H. Komiya, K. Masumoto, H. Y. Fan, *Phys. Rev.* **1964**, *133*, A1679–A1684.
[27] L. Bjerg, G. K. H. Madsen, B. B. Iversen, *Chem. Mater.* **2012**, *24*, 2111–2116.
[28] P. Jund, R. Viennois, X. Tao, K. Niedziolka, J.-C. Tédenac, *Phys. Rev. B* **2012**, *85*, 224105.

Received: August 24, 2020
Published Online: November 11, 2020